A Parametric Study of Flapped Airfoil Lift Enhancement by Vortex Generators

Natalie Souckova and Lukas Popelka
Institute of Thermomechanics, Academy of Sciences of the Czech Republic, Prague, CZ 182 00, Czech Republic
natalies@it.cas.cz, popelka@it.cas.cz

Milan Matejka
Department of Fluid Dynamics and Thermodynamics, FME, Czech Technical University in Prague, Prague, CZ 166 07, Czech Republic
Milan.Matejka@fs.cvut.cz

and

David Simurda
Institute of Thermomechanics, Academy of Sciences of the Czech Republic, Prague, CZ 182 00, Czech Republic
simurda@it.cas.cz

Presented at the XXX OSTIV Congress, Szeged, Hungary, 28 July - 4 August 2010

Abstract

This paper focuses on a suppression of the flow separation, which occurs on a deflected flap, by means of vortex generators (VGs). An NACA 63A421 airfoil with a simple flap and vane-type vortex generators was used. The investigation was carried out by using experimental and numerical methods. The data from the numerical simulation of the flapped airfoil without VGs control were used for the vortex generator design. Two different sizes and shapes, along with various spacing of the vortex generators, were tested. The flow past the airfoil was visualized with tuft filaments and oil-flow visualization. The experiments were performed in closed circuit wind tunnels with closed and open test sections. The lift curves for cases without and with vortex generators were acquired for the determination of the lift coefficient improvement. The improvement was achieved for several cases by means of all the applied methods.

Introduction

The principle of vortex generator flow control is based on generation of vortical structures, which transfer the high momentum fluid towards the surface. The flow with higher momentum can resist greater unfavorable pressure gradients. The reduction or suppression of flow separation and the related reduction in drag results in improved aerodynamic characteristics, less noise, heat transfer enhancement, etc. The vortex generators (VGs) can be of different shapes and sizes. The optimal VG position depends on flow parameters and flow separation location. This dependency limits the use of VGs to applications with relatively fixed location of flow separation. Because vortex generators are mounted in "pairs," the relative vortex generators placement in one pair influences the type of originating vortices, co-rotating or counter-rotating. The distance between the VGs also is important. Vortex generators are classified according to the ratio of VG height, h, and boundary layer height, δ, as conventional ($h/\delta > 0.5$), or low-profile ($0.1 < h/\delta < 0.5$). Due to the drag penalties of conventional VGs, the low-profile VGs are a subject of interest.

Considerable experimental research on the use of vortex generators for flow control has been performed. A comprehensive review of low-profile VGs focuses on basic research, as well as on airfoil and non-airfoil investigations.[1] However, there have not been many numerical simulations dealing with airfoil section applications. One of the few studies is concerned with passive and active flow separation control. Direct numerical simulation (DNS) was used and the vortex generator was modeled using the immersed-boundary method.[2] Unfortunately, there is a lack of solutions obtained by commercial codes, and those that are available focus on heat transfer in a channel.

The main subject of this work is the low-profile VG control of flow separation on a deflected simple flap of an NACA 63A421 airfoil. The investigation was carried out using experimental and numerical methods. In the first step, a non-control case was solved by means of numerical simulation to determine the location of flow separation and the boundary layer thickness. Information obtained from this calculation was utilized for VG design according to the best results of an earlier measurement, which dealt with vortex generator flow control on a bump,[3] and to the data for rectangular vane VG also used on the bump.[1] Then VGs were

applied to the flapped airfoil and their influence on the flow was investigated using tuft filaments and oil-flow visualization techniques. Furthermore, the flow control effectiveness in terms of the lift coefficient was evaluated from the pressure distribution measurements. All numerical simulations presented in this paper were carried out using the commercial code, Fluent. The entire research effort is described in following sections.

Vortex generator design

As is mentioned above, the first undertaking was a numerical simulation of the baseline without flow control. This baseline was an NACA 63A421 airfoil with a simple flap, deflected at zero and 20 degrees, and set at angles of attack from -5 to 15 degrees. The two-dimensional grid geometries were created in the program Gambit. Subsequently, the computational structured meshes were set up for all cases, as shown in Fig. 1. Solutions were obtained under the assumptions of steady, two-dimensional, incompressible viscous flow. Turbulence was modeled by two-equation k-ω Shear-Stress Transport (SST) model, so fully turbulent flow was expected. The inlet boundary conditions, which correspond to the boundary conditions of the experiment performed in Institute of Thermomechanics (IT), are defined using the Reynolds number, Re, the free stream velocity, v_∞, the turbulence intensity, Tu, and the length scale, L, the values of which are presented in Table 1. Symmetry conditions were set on the upper and bottom edges of the computational domain, the pressure-outlet boundary condition was defined at the outlet of the domain, and velocity-inlet boundary condition was used for the inlet part. A second-order, upwind discretization scheme was selected with respect to the mesh used.

The location of the separation point was identified from the x-component of the wall shear stress distribution over the upper surface of the geometry. The boundary condition for separation point is given by

$$\tau_w = 0 \qquad (1)$$

where τ_w is shear stress.

The separation point locations are summarized in Table 2. It is obvious that increasing of the angle of attack caused the separation point to move towards the leading edge at zero flap deflection. For the deflected flap case, however, the separation point moved slightly around the edge of the deflected flap up to an angle of attack of 5 degrees and, for higher angles, it also moved towards the leading edge.

The location of the separation points and the parameters defined in Table 3 were used as input data for the VG design. However, with regard to the small size of the airfoil model and the corresponding height of boundary layer, the VG heights and their distances from the separation points were determined while considering the manufacturing feasibility.

Experiments

The efficiency of the VGs to remove, or at least reduce, the presence of flow separation on a simple deflected flap, as well as their influence on the flow over the flap were observed using tufts and oil-flow visualization. In addition, their effect on the lift was found by integrating measured pressure distributions to determine lift coefficients as they depend on the angle of attack.

Wind tunnel, model, and vortex generators

Both pressure distribution measurement and tuft filament visualizations were carried out in the wind tunnel of the Department of Fluid Dynamics Laboratory of Institute of Thermomechanics, Academy of Sciences, Czech Republic. The closed circuit tunnel has a closed test section with dimensions of 865 mm x 485 mm x 900 mm. Angle of attack changes are enabled by electrically driven circular endplates.[4] Oil flow visualizations were performed in the wind tunnel of the Division of Fluid Dynamics Laboratory of FME, Czech Technical University in Prague. The closed circuit tunnel has an open test section with cross-section dimensions of 750 mm x 550 mm. The tunnel has a turbulence intensity of 3.5% at a free stream velocity of 16 m/s.

The NACA 63A421 airfoil having a simple flap was used. The model, having chord length 250 mm and span 485 mm, was fixed between two annular endplates made of transparent Plexiglas. The flap/chord ratio was 30%. The model was tested with a zero flap deflection and with a flap deflection of 20 deg.

Triangular and rectangular vane VGs were cut and formed from plastic sheet material. The VGs heights were chosen as 1.5 mm (small VG) and 3 mm (large VG) for both vane types. The other dimensions are given by the parameters in Table 3. The VGs were attached to the model surface such that the relative position of one vortex generator to the other within a pair was such that counter-rotating (CtR) vortices were produced, as shown in Figs. 2 and 3. Two spanwise rows of VGs were located at the non-dimensional chordwise locations, (x/c), of $x_1 = 0.5632$ and $x_2 = 0.65$ downstream of the leading edge. The distance of VGs from the separation points was not indicated because it changed with the angle of attack, as shown in Table 2. During the measurements, the spacing between VGs pairs was changed so that it either corresponded with parameters in Table 3, (Δz_1), or it was half of that value, (Δz_2). Low-profile VGs were mentioned earlier; however, there are some cases where the boundary-layer height is so small that a VG having the same height is no longer low-profile. This can happen due to the boundary layer height changing with angle of attack. Therefore, non low-profile VG cases are indicated.

All measurements were carried out at a Reynolds number of 200,000, and different ranges of angle of attack depending on the measurement technique used.

Tuft filaments visualization

Initially, the flow over the model without VGs was visualized to validate the numerical results, which showed the absence of laminar separation bubbles. To do this, the model was covered with tufts. The distance between tufts in each row depended on tuft length, which was set to avoid their mutual interference. After this, the tufts were kept only on the flap and visualization of the flow-controlled cases was performed, as shown in Fig. 4. The flow conditions indicated in Table 1 were maintained. The angle of attack range was from -5 to 15 degrees.

Oil-flow visualization

Owing to the unexpected results from the tuft observations, which are described in the Results and Discussion section in more detail, oil visualization was conducted for the zero angle of attack case. Initially, the measurement of the same non-controlled case was carried out and based on the observed separation bubble location, zig-zag tape was fixed to upper surface of the model at $x/c = 0.23$ downstream of the leading edge. Fully turbulent flow over most of the model was achieved, which led to separation bubble suppression. Thus, the measurements of the non-controlled as well as the controlled cases were performed with the tape in place. Since these measurements were not performed in the same wind tunnel as the previous one, the different turbulence intensity of the free stream flow must be noted.

Lift-curve measurement

The lift curve was obtained by integrating the measured pressure distributions to determine lift coefficients. The model with the zig-zag tape was used and cases with and without VGs were measured. The pressure orifices on side walls of the closed test section were employed to obtain the pressure distributions. Flow conditions were consistent with those of the tuft visualization experiments. The final lift curves for angles of attack ranging from –2.5 to 22.5 degrees include all of the necessary corrections.

Results and Discussion

The results from the tuft observations show that separation was suppressed on deflected flap only in the case of large rectangular VGs (x_1, Δz_2) at zero angle of attack, as can be seen in Figs. 5a and 5b. The flow separation on the airfoil without a flap deflection only appears at an angle of attack of 15 degrees, where separation started approximately in the middle of the chord, thus upstream of the VGs. Even though separation occurred upstream of the VGs, an improvement was still achieved with the large triangular VGs (x_1, Δz_2), as can be observed in Figs. 6a and 6b. In both of the cases noted here, the VGs used were of the conventional type. As these findings are not completely logical, oil-flow visualization was carried out.

The visualization for the clean model with and without a flap deflection was performed first, see Figs. 7a and 7b. A separation bubble is clearly observed in both of these cases. Thus, the tufts in this case were unsuited for displaying the separation bubble because either they affected the flow to cause boundary-layer transition, or they could not display the separation bubble because it was too small. The observations for the controlled case using tufts did not display distinctly how efficient the VGs were in suppressing flow separation on the deflected flap. In some cases, this is because the VGs were placed in the separation bubble which likely influenced their efficiency, especially for the low-profile ones.

As mentioned earlier, the zig-zag tape was used to avoid the situation described above. The subsequent oil-flow visualizations confirmed that the separation bubble was eliminated, and also displayed flow separation occurring near the trailing edge for the case without flap deflection and separated flow over the whole deflected flap, see Figs. 8a and 8b.

Next, the controlled cases were considered. It was found that the rectangular VGs had some effect in almost all cases. For the small (low-profile) VGs, there was a more significant influence at the position closer to the separation point, as presented in Figs. 9a and 9b, where downstream displacement of the separation point was achieved. The VGs effectiveness was better for larger spacing, as can be seen in Figs. 9b and 10. The large rectangular VGs (conventional) had considerable effect in all cases. The separation point shifted further downstream than it did for the small VGs, but the influence of the VG position from separation was not obvious (Figs. 11a and 11b). The triangular VGs did not have much effect on the separated flow except in the case of the large VGs (conventional, x_2, Δz_1), where only a slight influence was achieved, see Fig. 12.

The last experiment conducted was to obtain pressure distributions and the lift curve. The best results were obtained for conventional VGs, as was the case observed in the oil flow experiments. The largest lift coefficient increment was achieved for conventional, rectangular VGs (x_2, Δz_2). Also, the results for low-profile VGs were consistent with the oil-flow results; although there were some differences, mainly with the triangular, conventional VGs. The lift coefficient improvement was obtained with both positions of the triangular VGs, but they seemed to have little or no effect on the oil-flow results for these cases. From the lift curves, it also is evident that the range of the VGs effectiveness is up to an angle of attack of 10 degrees. For higher angles, the separation points occurred upstream of VGs and they no longer had an effect on the separated flow over the deflected flap, as can be seen in Figs. 13-15. The comparison of the lift curves for cases without a flap deflection showed an increment of lift coefficient for angles of attack from 5 to 15 degrees, except the conventional rectangular VGs (x_1, x_2, Δz_2), which showed a slight lift coefficient decrease, as can be seen in Fig. 16. These results correspond with those of the tuft observations.

Conclusions

This investigation brings some interesting findings and a few questions as well.

The flow separation over the deflected flap was not completely eliminated. However, the downstream movement of the separation point was achieved, particularly with conventional vortex generators (VGs). In addition, the rectangular vane VGs seemed to be more effective than the triangular ones for cases with a non-zero flap deflection. Also, it was found that the only improvement achieved with low-profile VGs was with the rectangular ones. In addition, the conventional VGs were not as sensitive to position changes as the low-profile VGs, because almost the same improvement was achieved for both positions using the large VGs, whereas the position played an important role in effectiveness of small ones.

The influence of spacing between VGs pairs is significant. Whereas large rectangular VGs had a more significant effect when employing the small spacing, the triangular ones had the opposite behavior. While it applies only to the large VGs, the larger spacing between conventional rectangular VGs pairs caused deterioration in the lift coefficient compared to the case with small spacing. It was observed in the oil-flow visualization experiments that the small rectangular VGs had the same effect as triangular ones.

The questions that are introduced by the results obtained are the big differences in the effectiveness between the rectangular and triangular VGs, as well as with particular VGs behavior as the spacing changed. Thus, future work will use flow visualization to help better understand differences in the vortices produced by pairs of vortex generators. In addition, numerical simulations of VG control on a deflected flap will continue. Future work also will focus on drag force measurements to determine the drag penalties of VGs, as well as for the validation of numerical simulations.

Acknowledgments

The work has been supported by Ministry of Education, Youth and Sports of the Czech Republic within project No. 1M06031. Support by the Czech Science Foundation under grants No. IAA2076403 and No. GA 101/08/1112 is gratefully acknowledged.

References

[1]Lin, J.C., "Review of research on low-profile vortex generators to control boundary-layer separation," Progress in Aerospace Science 38, 2002, pp. 389-420.

[2]Shan H., Jiang L., Liu C., Love M., Maines B., "Numerical study of passive and active flow separation control over a NACA0012 airfoil," Computer & Fluids 37, 2008, pp. 975-992.

[3]Godard G., Stanislas M., "Control of a decelerating boundary layer. Part 1: Optimization of passive vortex generator," Aerospace Science and Technology 10, 2006, pp. 181-191.

[4]Popelka L., "Wind Tunnel Test Section for Airfoils and Bodies, Research Programme Feasibility Studies," Conference Topical Problems of Fluid Mechanics, Institute of Thermomechanics AS CR, Prague, 2008, pp. 85-88.

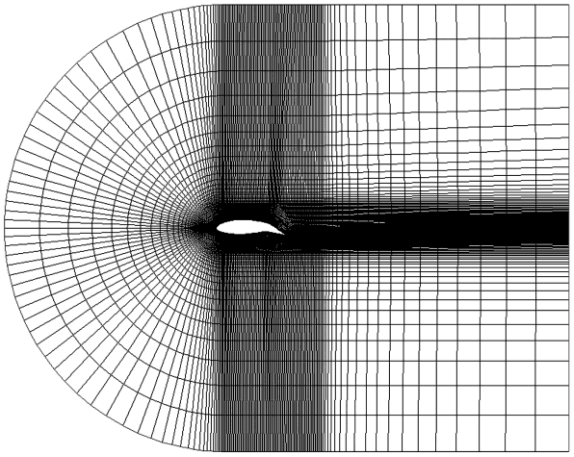

Figure 1 Computational mesh.

Table 1
Inlet boundary conditions

v_∞, m/s	Tu, %	L, m	Re
12	0.25	0.005	200,000

Table 2
Non-dimensional flow separation locations x/c for range of angles of attack α, with and without flap deflection γ

	γ, deg.	
α, deg.	0	20
-5	0.9653	0.7429
0	0.9195	0.7476
5	0.7910	0.7385
10	0.6036	0.5569
15	0.4323	0.4330

Table 3
Vortex generators design parameters

		VGs	h/δ	$\Delta X_{VG}/h$	e/h	L/h	Δz/h	β, deg.
Godard 2006	CtR	Trinagular vanes	0.37	57	2	2.5	6	18
Lin 2008	CtR	Rectangular vanes	0.2	10	4	-	9	25

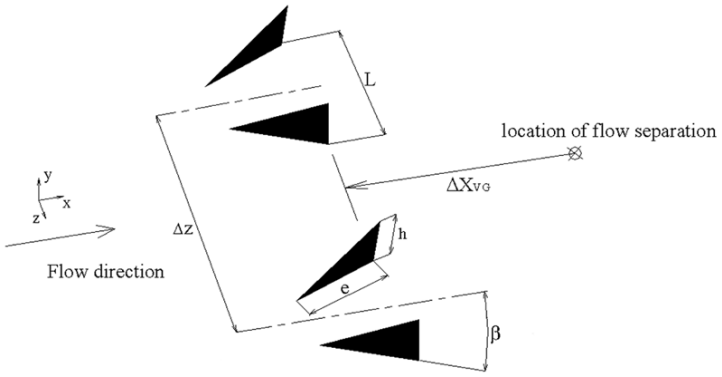

Figure 2 Triangular VGs and their relative positions.

Figure 3 VGs location on upper surface of the model.

Figure 4 Tuft filaments placement on the deflected flap.

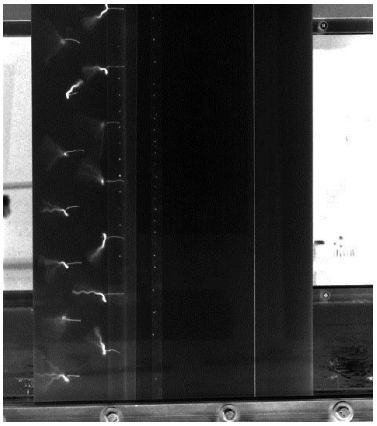

a)

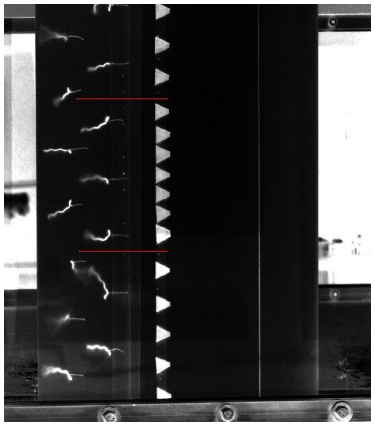

b)

Figure 5 Tuft filaments visualization of the non-controlled case, with flap deflection of 20 deg., α = 0 deg. (the free stream flow direction is from right to left). Controlled case (conventional rectangular VGs, x_1, Δz_2) with flap deflection of 20 deg., α = 0 deg. (the free stream flow direction is from right to left).

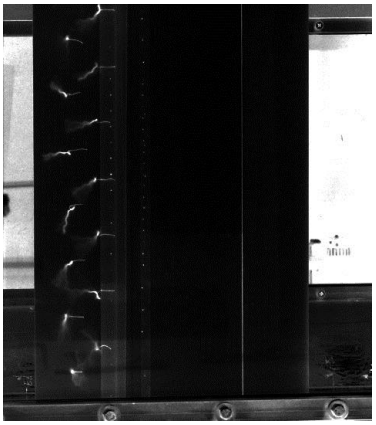

a)

Figure 6 Tuft filaments visualization of the non-controlled case, without flap deflection, α = 15 deg. (the free stream flow direction is from right to left).

b)

Controlled case (conventional triangular VGs, x_1, Δz_2) without flap deflection, α = 15 deg. (the free stream flow direction is from right to left).

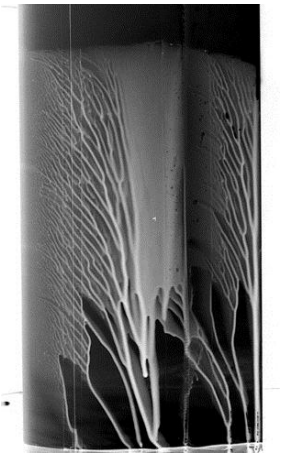

a)

Figure 7 Oil visualization of the non-controlled case without flap deflection (the free stream flow direction is from left to right).

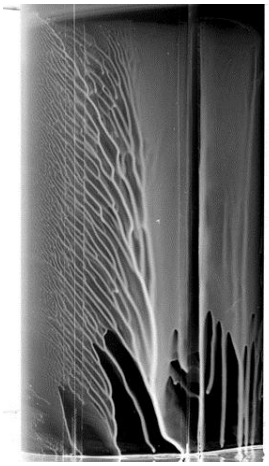

b)

Oil visualization of the non-controlled case with flap deflection of 20 deg. (the free stream flow direction is from left to right).

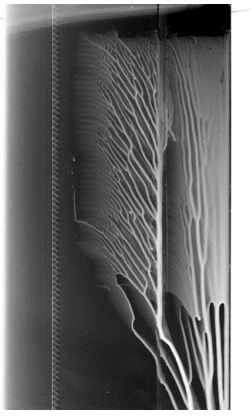

a)

Figure 8 Oil visualization for the case with VGs, with zig-zag tape at x/c = 0.23 and without flap deflection (the free stream flow direction is from left to right).

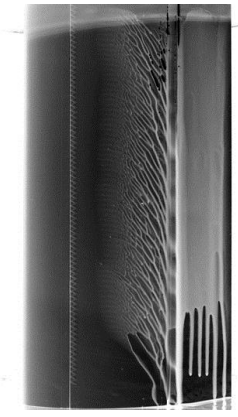

b)

Oil visualization of case with VGs, with zig-zag tape at x/c = 0.23 and with flap deflection of 20 deg. (the free stream flow direction is from left to right).

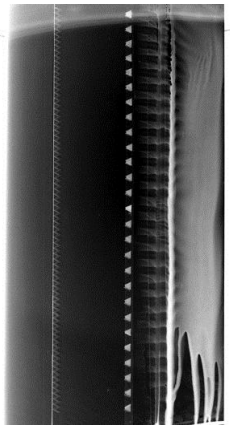

a)

Figure 9 Oil visualization of the controlled case (low-profile rectangular VGs, x_1, Δz_1), with zig-zag tape and with flap deflection (the free stream flow direction is from left to right).

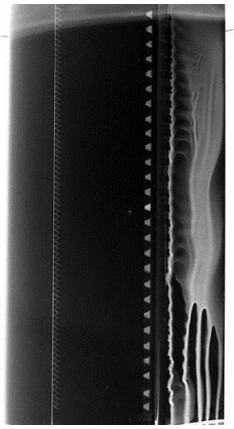

b)

Oil visualization of the controlled case (low-profile rectangular VGs, x_2, Δz_1), with zig-zag tape and with flap deflection (the free stream flow direction is from left to right).

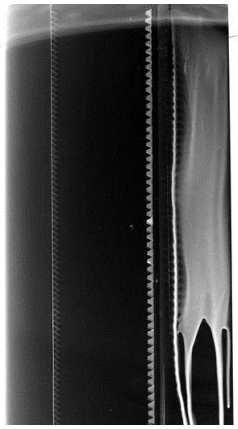

Figure 10 Oil visualization of the controlled case (low-profile rectangular VGs, x_2, Δz_2), with zig-zag tape and with flap deflection (the free stream flow direction is from left to right).

a)

Figure 11 Oil visualization of the controlled case (conventional rectangular VGs, x_1, Δz_2), with zig-zag tape and with flap deflection (the free stream flow direction is from left to right).

b)

Oil visualization of the controlled case (conventional rectangular VGs, x_2, Δz_2), with zig-zag tape and with flap deflection (the free stream flow direction is from left to right).

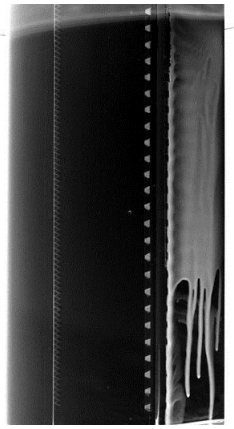

Figure 12 Oil visualization of the controlled case (conventional triangular VGs, x_2, Δz_1), with zig-zag tape and with flap deflection (the free stream flow direction is from left to right).

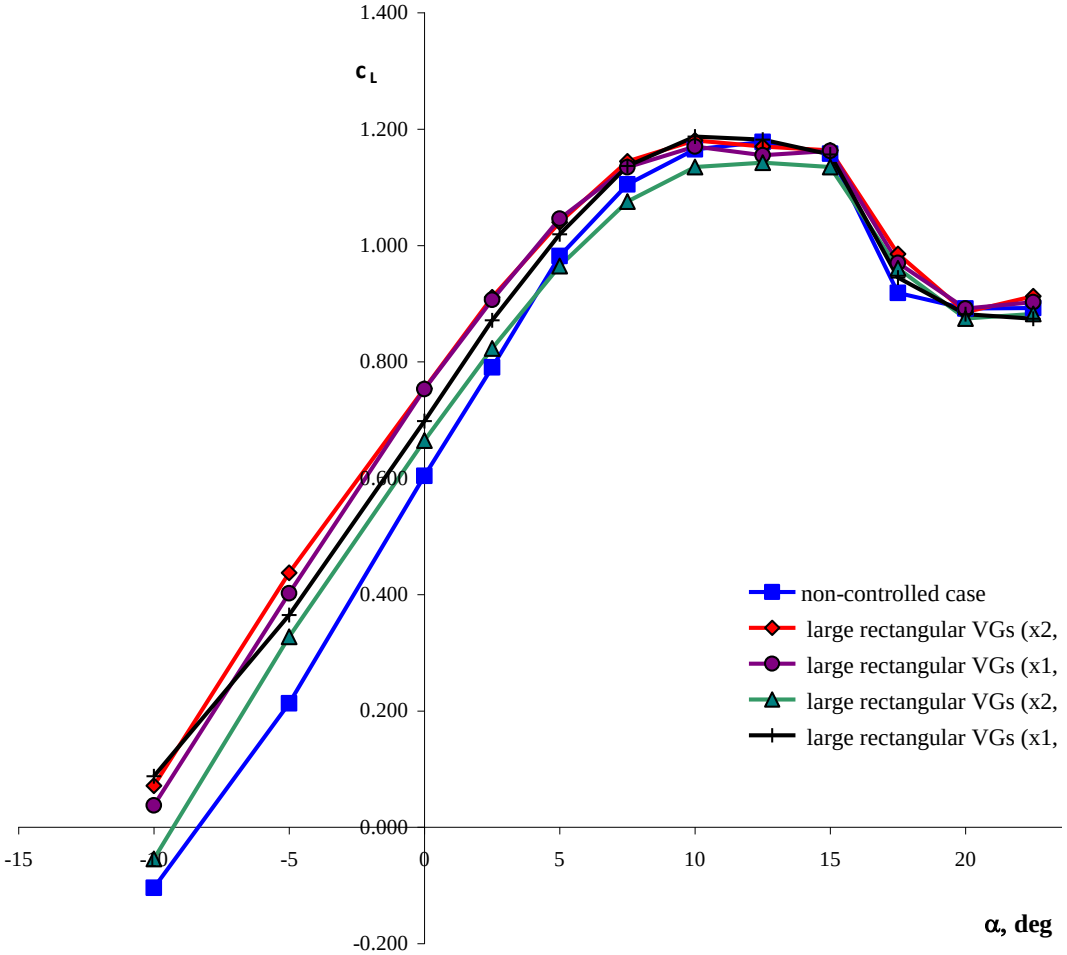

Figure 13 Lift slopes comparison of the non-controlled and controlled cases with conventional rectangular VGs at the flap deflection of 20 deg.

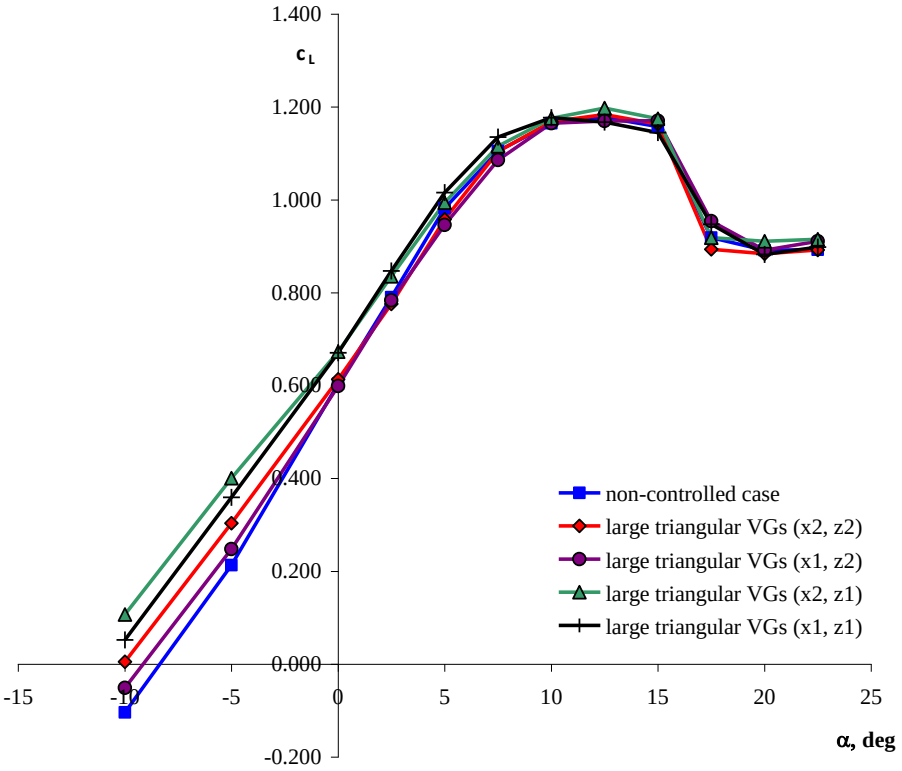

Figure 14 Lift slopes comparison of the non-controlled and controlled cases with conventional triangular VGs at the flap deflection of 20 deg.

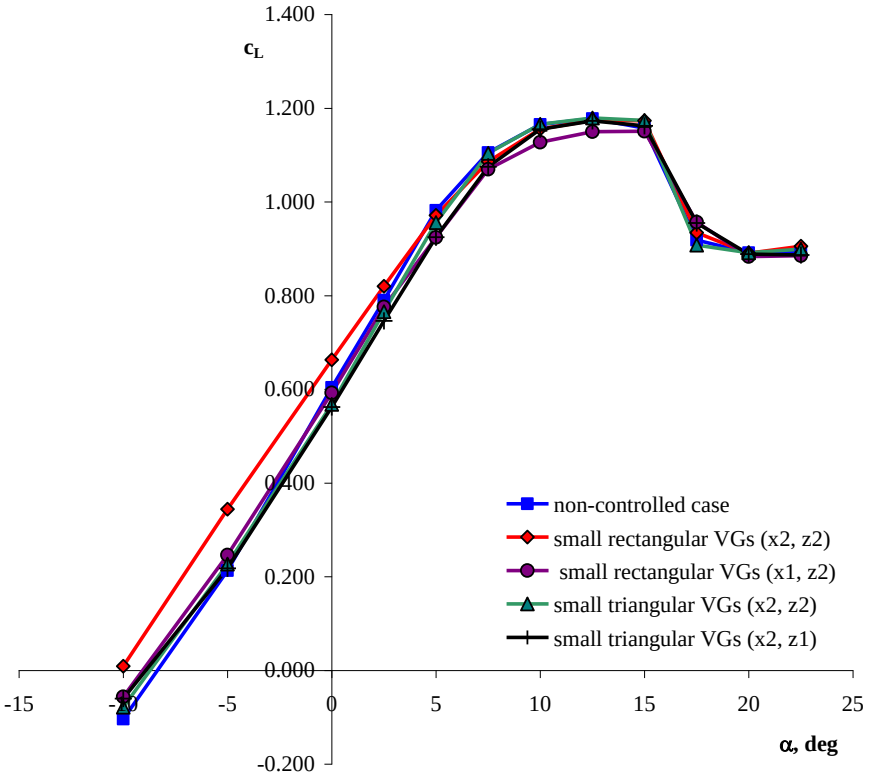

Figure 15 Lift slopes comparison of the non-controlled and controlled cases with low-profile VGs at the flap deflection of 20 deg.

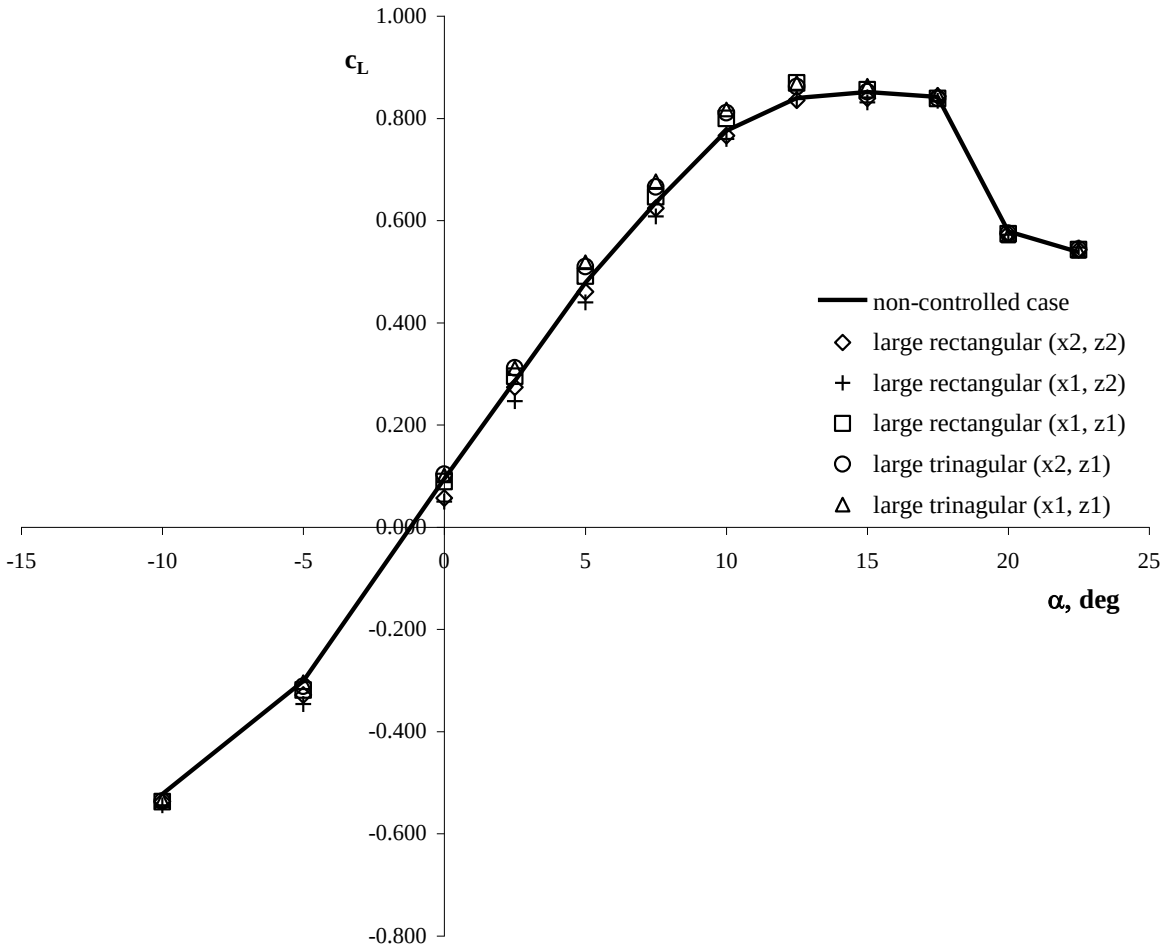

Figure 16 Lift slopes comparison of the controlled cases with the largest lift coefficient increment at flap deflection of 20 deg. at the flap deflection of 0 deg.